Communication

Watching Nanoparticles Grow: The Mechanism and Kinetics for the Formation of TiO-Supported Platinum Nanoparticles

Peter J. Chupas, Karena W. Chapman, Guy Jennings, Peter L. Lee, and Clare P. Grey

J. Am. Chem. Soc., **2007**, 129 (45), 13822-13824• DOI: 10.1021/ja076437p • Publication Date (Web): 23 October 2007

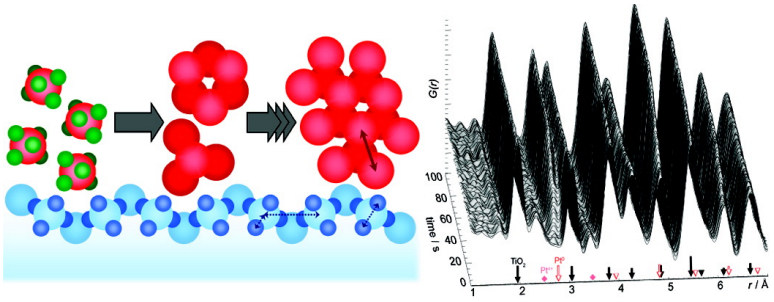

More About This Article

Additional resources and features associated with this article are available within the HTML version:

- Supporting Information
- Links to the 2 articles that cite this article, as of the time of this article download
- Access to high resolution figures
- Links to articles and content related to this article
- Copyright permission to reproduce figures and/or text from this article

View the Full Text HTML

J|A|C|S
COMMUNICATIONS

Published on Web 10/23/2007

Watching Nanoparticles Grow: The Mechanism and Kinetics for the Formation of TiO_2-Supported Platinum Nanoparticles

Peter J. Chupas,*,† Karena W. Chapman,*,† Guy Jennings,† Peter L. Lee,† and Clare P. Grey*,‡

X-ray Science Division, Advanced Photon Source, Argonne National Laboratory, Argonne, Illinois 60439, and Department of Chemistry, Stony Brook University, Stony Brook, New York 11794-3400

Received August 27, 2007; E-mail: chupas@anl.gov; chapmank@aps.anl.gov; cgrey@notes.cc.sunysb.edu

Highly dispersed supported metal nanoparticles find widespread application in catalysis, including in hydrocarbon reforming and polymer-electrolyte-membrane fuel cells.[1−8] Pivotal to the development of catalytic materials with controlled reactivity is the understanding of the fundamental mechanisms that drive the formation of catalytic nanoparticles. A key step toward this goal is the ability to discriminate between the separate processes, including the initial reaction of the precursors and the subsequent nanoparticle sintering. Recently, the pair distribution function (PDF) method has emerged as a powerful technique to probe the structure of nanoscale materials, with atomic-scale resolution across the entire length scale of the nanoparticle, although to date this has been limited to studies of static materials prepared ex situ, such as in advance of the measurement.[9−12] Here we use in situ time-resolved PDF methods to monitor the structural evolution and kinetics associated with the formation of Pt^0 nanoparticles from Pt^{4+} ions. Differential PDF (d-PDF) methods are applied, which allow the atom−atom correlations that arise only from the supported Pt material (i.e., metal−metal and metal−anion contacts) to be separated from those of the bulk support, TiO_2, to probe the structure of the nanoparticles directly. We demonstrate that the reduction reaction follows pseudo-zero-order kinetics. The mobility of the Pt atoms on the TiO_2 support varies with temperature, with particle growth proceeding more rapidly at higher temperatures.

The potential of X-ray and neutron PDF methods to solve problems in catalysis has been demonstrated for industrially relevant zeolites and supported Pt systems.[8,13,14] Although innovative at the time, these studies, were limited by the flux, with each PDF requiring several hours to a week of collection time. The use of synchrotron radiation in combination with an area detector[15] allows the scattering data for an individual PDF to be collected simultaneously such that the time resolution is limited only by the flux/signal-to-noise ratio and the data read-out rate. Here, the application of a highly sensitive, fast read-out detector[16] has allowed structural and mechanistic information to be obtained with time resolutions up to 133 ms. This represents a significant advance in the study of nanoparticles, as it opens up the new possibility of probing structure with sufficient time resolution to directly distinguish the reactions of the precursors from that involving particle growth.

The present approach offers several distinct advantages over the X-ray absorption spectroscopy (XAS) methods more typically used to characterize supported nanoparticles. The monochromatic high-energy X-rays (>60 keV) used for PDF measurements are weakly absorbing, causing negligible radiation damage or perturbation to the sample—a particular problem for time-resolved XAS (energy dispersive EXAFS) which uses X-ray energies close to an absorption edge.[17,18] Unlike EXAFS data, the d-PDFs (and PDFs) contain structural information beyond the first few coordination shells, to longer length scales (≫10 Å), providing insight into the size and morphology of the nanoparticles. The bond lengths obtained from the PDF are absolute, not subject to an offset or derived from a structural model, as is typical for distances "measured" in an EXAFS experiment.

The Pt^{4+} reduction kinetics, preceding nanoparticle formation, were probed by following the reaction of $PtCl_6^{2+}$ ions supported on TiO_2, at multiple temperatures. Starting materials were prepared by aqueous deposition of H_2PtCl_6 on TiO_2 with 5 wt % Pt loading. High-energy X-ray scattering data ($\lambda = 0.1612$ Å) were collected at 1-ID-C at the Advanced Photon Source for polyimide capillary-loaded Pt^{4+}/TiO_2 samples in a reaction cell which allows rapid gas switching near the sample. Diffraction images were accumulated using an amorphous silicon-based area detector[16] during sample reduction under H_2 (4% in He) gas flow at three temperatures, 100, 150, and 200 °C.

The PDFs, $G(r)$, obtained during the reduction (Figure 1) were extracted from the diffraction images as described previously.[15] The PDFs contain contributions from all atom−atom correlations within the sample, including those from the majority TiO_2 support and the deposited Pt species. The TiO_2 correlations remain unchanged during reduction, while those from the Pt^0 nanoparticles increase and those from the precursor decrease.

While direct analysis of the minority Pt^{4+}/Pt^0 component is complicated by the dominant contribution of the support to the total PDF, it can be readily analyzed in the d-PDF (Figure 2). These d-PDFs were obtained by direct subtraction of a reference PDF measured for the bare support (at the same temperature) from the total PDFs, renormalized to the Ti−O correlation (2.0 Å).

The d-PDF of the as-deposited sample has a distinct correlation at 2.5 Å corresponding to the Pt−Cl bond within the $PtCl_6^{2-}$ anion. A peak due to the Pt−Pt nearest-neighbor correlation develops rapidly at 2.77 Å during the reaction. The relative intensities of these first shell Pt−Cl precursor and Pt−Pt product correlations, estimated from Gaussian fits to the peaks, change during the reaction, reflecting changes in species concentration and coordination number (Figure 3). The intensity of the Pt−Cl correlation, from the discrete $PtCl_6^{2-}$ ion, is directly proportional to the concentration of Pt−Cl bonds and $PtCl_6^{2-}$ ions and, thus, provides a direct measure of the progress of reduction. By contrast, the intensity of the Pt−Pt correlation and number of Pt−Pt contacts depend on the concentration of Pt^0 species as well as the size/extent of the particle, and thus, this correlation (particularly in comparison to the Pt−Cl correlation) can provide additional information regarding particle formation and growth.

No induction time is evident for the reduction at 100−200 °C, the Pt−Cl correlation decreasing approximately linearly with reaction time (Figure 3). The lack of induction time indicates that the reduction is not autocatalytic, as has been found for Pt^{4+} species in solution.[20] Tests of zero-order and first-order kinetic models

† Argonne National Laboratory.
‡ Stony Brook University.

10.1021/ja076437p CCC: $37.00

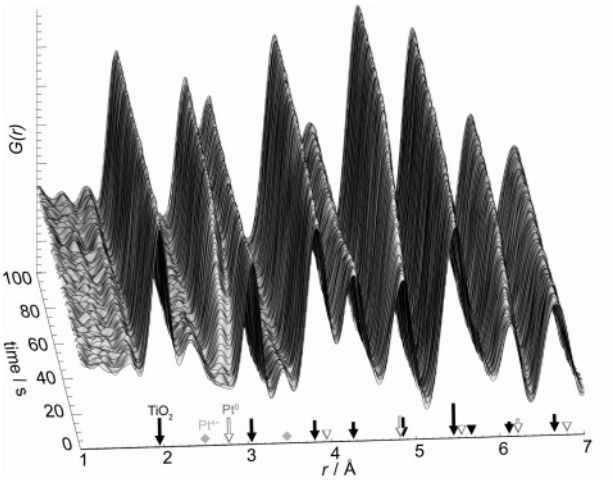

Figure 1. Total PDFs, $G(r)$, for Pt/TiO_2 during reduction at 200 °C. Arrows indicate correlations arising from TiO_2, Pt^{4+}, and Pt^0 species.

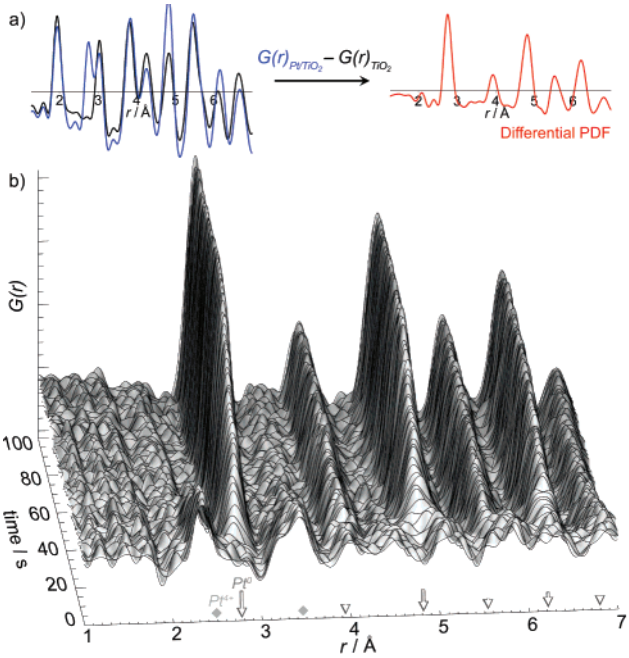

Figure 2. (a) Recovery of the d-PDF isolating correlations involving only Pt. (b) A series of d-PDFs for Pt/TiO_2 during reduction at 200 °C.

suggest that the data are better fit by a zero-order model ($R^2_{\text{zero-order}} = 0.94-0.98$, $R^2_{\text{first-order}} = 0.84-0.90$). Small deviations from a perfect linear fit may be due to a contribution from a secondary process which follows different kinetic behavior. XAS studies have indicated that reduction of supported Rh follows first-order kinetics, although different kinetics may be reasonably expected for different systems.[21] Indeed, interpretation of XAS data can be complicated by multiple scattering effects and may be influenced by cluster size effects and the absolute number of species present.[22] While generally considered rare, zero-order kinetics often apply to reactions at surfaces with a fixed number of catalytic reaction sites (e.g., defects).[23] In supported systems, such as Pt/TiO_2, the surface area to volume ratio is considerably larger than that of a bulk precursor, and as such, the reduction process may be dominated by existing surface defect/reaction sites. Accordingly, zero-order kinetic behavior analogous to that of surface-catalyzed reactions may be reasonably anticipated.

The activation energy for the reduction of a nanoparticle is generally challenging to measure experimentally and even more

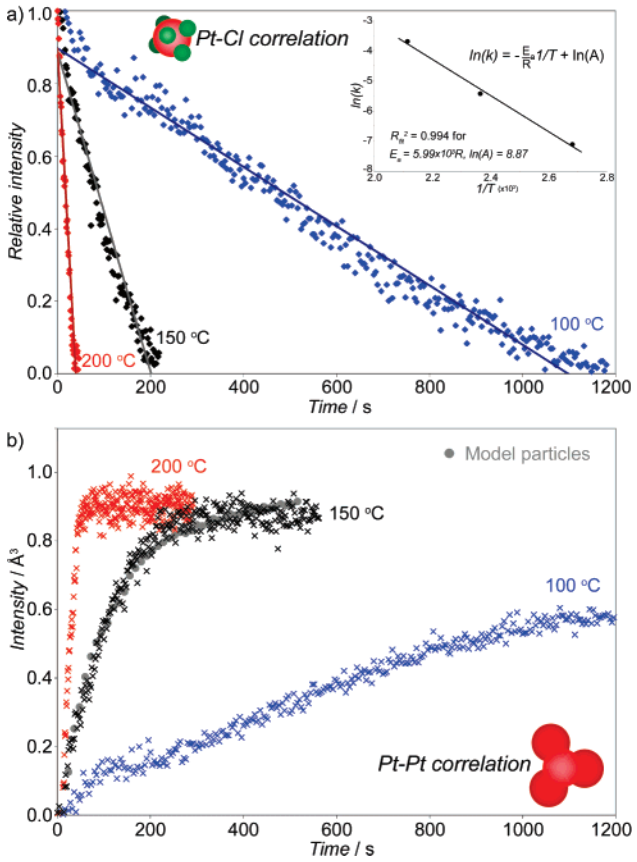

Figure 3. The first shell Pt−Cl (a) and Pt−Pt (b) peak intensities during reduction at 100, 150, and 200 °C and the corresponding Arrhenius plot (inset). The trend expected for linear growth (by mass) of hypothetical nanoparticles is superimposed on the data obtained at 150 °C.

so for heterogeneous systems. This energy can, however, be recovered readily from an Arrhenius plot, based on the zero-order fits to the PDF data, resulting in a value of 0.52 eV (Figure 3).

The first shell Pt−Pt peak grows continuously as clusters of several atoms grow to form small particles, with the average coordination number (CN) increasing and eventually approaching that of bulk Pt (CN = 12) on heating at 150 °C and above. The linear decrease in the Pt−Cl correlation and the zero-order reduction kinetics suggest a linear increase in Pt^0 species; thus, the growth in the first shell Pt−Pt peak intensity corresponding to linear growth (by mass or number of atoms) of the clusters was calculated (Figure 3). These calculations demonstrate that linear growth of a single particle, or linear parallel growth of multiple identical particles, is associated with nonlinear increase in the first shell Pt−Pt intensity. To a first approximation, this parallels the observed behavior; however, small deviations from the calculated growth curves suggest that other processes may influence the rate of Pt−Pt bond formation (including migration/mobility of Pt^0 atoms and clusters, and the rate of addition of a Pt atom to another atom or small cluster). A distribution of particle sizes, nucleated over a period of times, at various stages of particle growth is also likely. Comparison of the relative rates and completeness of the Pt−Pt bond and Pt^0 formation shows that Pt particle growth depends strongly on temperature, with growth at 100 °C likely limited by reduced mobility of Pt^0 atoms.

To further explore the effect of temperature on the relative rates of the two processes, data were collected at ~3 K intervals as the Pt^{4+}/TiO_2 was heated, under H_2 (4% in He) gas flow, from 0 to 200 °C over 1 h then held at 200 °C for 15 min. The changes in intensity of the Pt−Cl and Pt−Pt correlations indicate several

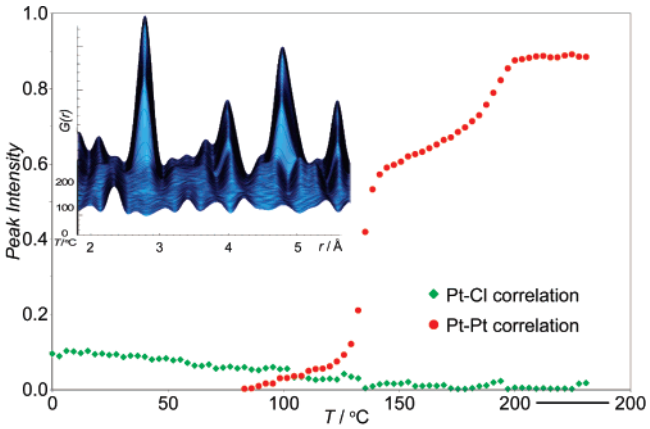

Figure 4. The d-PDFs (inset) and the integrated peak intensities of the Pt−Cl and Pt−Pt correlations upon heating under H_2 (4% in He) gas flow.

distinct behaviors (Figure 4). Between 0 and 125 °C, the dominant reaction involves the reduction of Pt^{4+} to form isolated Pt^0 atoms or small clusters, as evident from the substantial drop of the Pt−Cl correlation intensity and only a significantly smaller growth of the peak due to Pt−Pt contacts. At 125−140 °C, the intensity of the Pt−Pt correlation grows dramatically without any significant changes for the Pt−Cl correlation. Thus, the increase in Pt−Pt intensity and Pt CN derives from particle growth and sintering rather than a rapid increase in the number of Pt^0 species. Above 140 °C, a more gradual increase in the Pt−Pt correlation is observed. At this temperature, the reduction of the Pt^{4+} is complete, as evident by the lack of Pt−Cl contacts, and this increase of the Pt−Pt correlation is due to further growth of the Pt nanoparticles through the slower merging of larger particles with other (smaller) clusters. An estimate of the Pt coordination number calculated from the Pt−Pt correlation intensity (see Supporting Information) is consistent with this, the average CN increasing by ∼2.5 from <6 to 8.5 at 125−140 °C, and by a further ∼2.5 to ∼11 from 140 to 200 °C. A further measure of particle size can be obtained from the distance *r* to which distinct correlations in the PDF remain since peaks will not be evident beyond the length scale of the particle.[24] On the basis of this analysis, the particles have grown to over 5 nm at 200 °C. These results indicate a dramatic increase in the mobility of Pt atoms or small clusters on the TiO_2 support above ∼125 °C, consistent with the isothermal results.

Variations in d-PDF peak positions and shapes during the reaction (Figure 4) indicate additional subtleties associated with cluster formation and growth mechanisms. The data suggest that the structure of some clusters may not resemble that of bulk face-centered cubic (fcc) Pt. The first shell Pt−Pt correlation is broad and slightly asymmetric below ∼125 °C, consistent with a distribution of Pt−Pt bond lengths, and perhaps multiple cluster types. Above ∼125 °C, the first shell peak sharpens and the splitting of the third shell peak disappears, as the particles grow in size. Concomitantly, the peaks shift to lower *r* due to a contraction of the Pt−Pt bond with heating. Such negative thermal expansion has been observed in Pt particles of less than a nanometer,[19] again indicating that small clusters/particles (<1 nm) are present in this temperature regime. By 200 °C, where the small clusters/particles have sintered into larger particles of ∼5 nm, the long-range correlations in the PDF are now well reproduced by a fcc model. Grazing incidence small-angle X-ray scattering (GISAXS) studies are now planned to further characterize the size and shape of the initial metal clusters in situ.[5]

In conclusion, we illustrate a methodology for the direct and quantitative study of the kinetics and mechanism of nanoparticle formation and sintering in heterogeneous systems, an area that has been largely overlooked, due to a lack of adequate experimental methodology. The advantage of the present approach is that it directly discriminates between the reactions involving the precursor and those involving sintering and particle growth. The methods described here are not limited to Pt nanoparticles but are broadly applicable to the study of both the chemical kinetics associated with nanoparticle formation and the stability of nanoparticles under reaction conditions. Applications of this approach to a large variety of systems, including nanocomposites in lithium ion battery materials and supercapacitors, iron-oxyhydroxide nanoparticles in the environment, and gold nanoparticles in catalysis, can be readily envisaged.

Acknowledgment. Work performed at Argonne National Laboratory was supported by the U.S. DOE, Office of Science, Office of Basic Energy Sciences, under Contract No. DE-AC02-06CH11357. C.P.G. acknowledges financial support provided by the DOE through grant DE-FG02-96ER14681.

Supporting Information Available: Details of diffraction experiment, PDF refinements, ex situ PDF data, and calculations of average coordination numbers. This material is available free of charge via the Internet at http://pubs.acs.org.

References

(1) Thomas, J. M.; Johnson, B. F. G.; Raja, R.; Sankar, S.; Midgley, P. A. *Acc. Chem. Res.* **2003**, *36*, 20−30.
(2) Russell, A. E.; Rose, A. *Chem. Rev.* **2004**, *104*, 4613−4365.
(3) Argo, A. M.; Odzak, J. F.; Gates, B. C. *J. Am. Chem. Soc.* **2003**, *125*, 7107−7115.
(4) Guzman, J.; Carrettin, S.; Fierro-Gonzalez, J. C.; Gates, B. C.; Corma, A. *Angew. Chem., Int. Ed.* **2005**, *44*, 4778−4781.
(5) Winans, R. E.; Vajda, S.; Lee, B.; Riley, S. J.; Seifert, S.; Tikhonov, G. Y.; Tomczyk, N. A. *J. Phys. Chem. B* **2004**, *108*, 18105−18107.
(6) Rhodes, H. E.; Wang, P.; Stokes, H. T.; Slichter, C. P.; Sinfelt, J. H. *Phys. Rev. B* **1982**, *26*, 3559−3568.
(7) Thomas, J. M.; Midgley, P. A. *Chem. Commun.* **2004**, *11*, 1253−1267.
(8) Gallezot, P.; Bergeret, G. *J. Catal.* **1981**, *72*, 294.
(9) Billinge, S. J. L.; Levin, I. *Science* **2007**, *316*, 561−565.
(10) Michel, F. M.; Ehm, L.; Antao, S. M.; Lee, P. L.; Chupas, P. J.; Liu, G.; Strongin, D. R.; Schoonen, M. A. A.; Philips, B. L.; Parise, J. B. *Science* **2007**, *316*, 1726−1729.
(11) Egami, T.; Billinge, S. J. L. In *Underneath the Bragg Peaks: Structure Analysis of Complex Materials*; Cahn, R., Ed.; Oxford/Pergamon Press: New York, 2004.
(12) Rolison, D. R. *Science* **2003**, *299*, 1698−1701.
(13) (a) Shannon, R. D.; Gardner, K. H.; Staley, R. H.; Bergeret, G.; Gallezot, P.; Auroux, A *J. Phys. Chem.* **1985**, *89*, 4778−4788. (b) Martinez-Inesta, M. M.; Lobo, R. F. *J. Phys. Chem. C* **2007**, *111*, 8573−8579.
(14) Eckert, J.; Draznieks, C. M.; Cheetham, A. K. *J. Am. Chem. Soc.* **2002**, *124*, 170−171.
(15) Chupas, P. J.; Qiu, X.; Hanson, J. C.; Lee, P. L.; Grey, C. P.; Billinge, S. J. L. *J. Appl. Crystallogr.* **2003**, *36*, 1242−1247.
(16) Chupas, P. J.; Chapman, K. W.; Lee, P. L. *J. Appl. Crystallogr.* **2007**, *40*, 463−470.
(17) Newton, M. A.; Dent, A. J.; Evans, J. *Chem. Soc. Rev.* **2002**, *31*, 83−95.
(18) Mesu, J. G.; van der Eerden, A. M. J.; de Groot, F. M. F.; Weckhuysen, B. M. *J. Phys. Chem. B* **2005**, *109*, 4042−4047.
(19) Kang, J. H.; Menard, L. D.; Nuzzo, R. G.; Frenkel, A. I. *J. Am. Chem. Soc.* **2006**, *128*, 12068−12068.
(20) Besson, C.; Finney, E. E.; Finke, R. G. *J. Am. Chem. Soc.* **2005**, *127*, 8179−8184.
(21) Newton, M. A.; Fiddy, S. G.; Guilera, G.; Jyoti, B.; Evans, J. *Chem. Commun.* **2005**, 118−120.
(22) Ankudinov, A. L.; Rehr, J. J.; Low, J. J.; Bare, S. R. *J. Synchrotron Radiat.* **2001**, *8*, 578−580.
(23) Williams, C. T.; Chen, E. K.-Y., Takoudis, C. G.; Weaver, M. J. *J. Phys. Chem. B* **1998**, *102*, 4785−4796.
(24) Page, K.; Proffen, T.; Terrones, H.; Lee, L.; Yang, Y.; Stemmer, S.; Seshadri, R.; Cheetham, A. K. *Chem. Phys. Lett.* **2004**, *393*, 385−388.

JA076437P